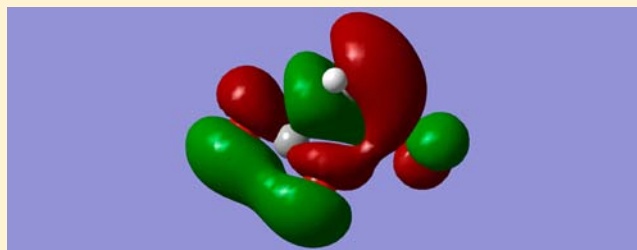# Decomposition of Malonic Anhydrides

Charles L. Perrin,* Agnes Flach, and Marlon N. Manalo[†]

Department of Chemistry, University of California—San Diego, La Jolla, California 92093-0358, United States

S *Supporting Information*

ABSTRACT: Malonic anhydrides decompose at or below room temperature, to form a ketene and carbon dioxide. Rate constants for the thermal decomposition of malonic, methylmalonic, and dimethylmalonic anhydrides were measured by NMR spectroscopy at various temperatures, and activation parameters were evaluated from the temperature dependence of the rate constants. Methylmalonic anhydride is the fastest, with the lowest $\Delta H^{\ddagger}$, and dimethylmalonic anhydride is the slowest. The nonlinear dependence on the number of methyl groups is discussed in terms of a concerted $[2_s + (2_s + 2_s)]$ or $[2_s + 2_a]$ cycloreversion that proceeds via a twisted transition-state structure, supported by computations.

INTRODUCTION

Until 1978, malonic anhydrides (2,4-oxetanediones, according to *Chemical Abstracts*) were classic unknown substances, the goals of 70 years of synthetic attempts. Although heating a succinic or glutaric acid with a dehydrating agent converts either of these to its anhydride,[1] this simple synthetic route fails to give malonic anhydride. Instead, carbon suboxide, O=C=C=C=O, is produced.[2] Furthermore, dehydration (or other transformation)[3] of a substituted malonic acid derivative leads to oligomeric or polymeric anhydrides.[4] Clearly, the challenge to the formation of the monomeric form is the strained four-membered ring. Indeed, the (calculated) enthalpy of hydrolysis of malonic anhydride is −134 kJ·mol⁻¹, considerably more exothermic than the −53 kJ·mol⁻¹ of succinic anhydride.[5] In contrast, a malonoyl peroxide, with a five-membered ring, is readily accessible and is effective as a reagent for dihydroxylation of alkenes.[6]

Malonic anhydrides were at last synthesized by Perrin and Arrhenius.[7] The key to success was to start with an already formed four-membered ring, as shown in Scheme 1. Ozonolysis

Scheme 1. Synthesis of Malonic Anhydrides 2
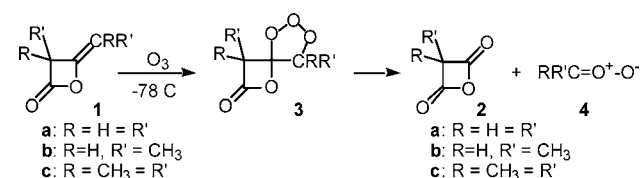
of the enol-lactone dimer (1) of a ketene at −78 °C produces the malonic anhydride (2). According to model studies on isopropenyl acetate and 6-phenyl-5-hydroxy-5-hexenoic acid δ-lactone, cleavage of the molozonide (3) occurs so that the extra oxygen of ozone is acquired by the aldehyde, not by the anhydride. The resulting carbonyl oxide (4) can be trapped

with *N*-methylmorpholine *N*-oxide,[8] or with benzaldehyde to form an ozonide (*Caution!*),[9] or it can be allowed to dimerize, trimerize, or oligomerize, to form peroxides (*Caution!*). Nevertheless, regardless of the fate of the carbonyl oxide byproduct, the malonic anhydride itself is produced by this simple procedure. Its structure was characterized by derivatization and spectroscopically,[10] especially by an IR band at 1820 cm⁻¹ and a Raman band at 1947 cm⁻¹, which is a champion among organic C=O frequencies.[11]

Malonic anhydrides are useful materials that can be easily derivatized to a variety of monoesters and monoamides[12] that are commonly used in the synthesis of pharmaceuticals, natural products, and other biologically active compounds.[13] Another proposed application is the production of Meldrum's acid,[14] which is useful in organic synthesis.[15]

The aspect of malonic anhydrides addressed here is their decomposition. The products are carbon dioxide and a ketene (5 in Scheme 2), as has also been observed for a

Scheme 2. Decomposition of Malonic Anhydrides
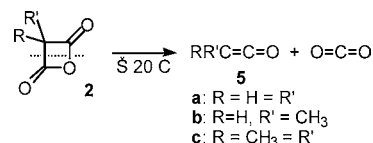
methylenemalonic anhydride.[16] Decomposition occurs near or below room temperature; this explains why they eluded synthesis for so long and demonstrates the advantage of an ozonolytic synthesis, which can be performed at −78 °C. But why is decomposition so fast? Also, why does the parent malonic anhydride (2a, R = H = R′) decompose at a lower

temperature than does dimethylmalonic anhydride (**2c**, R = CH$_3$ = R′), even though a faster reaction might have been expected for the latter (by weak analogy to the Saytzeff rule for β-eliminations,[17] due to stabilization of the more highly alkylated alkene)?

This decomposition is unquestionably a [2 + 2] cyclo-reversion. Because a [2$_s$ + 2$_s$] cycloreversion is forbidden, this reaction has been considered to be a [2$_s$ + 2$_a$] process, via a twisted transition-state structure, as illustrated in Figure 1a.
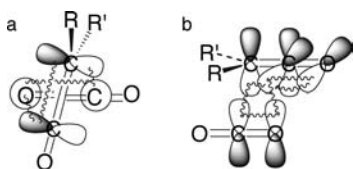

Figure 1. Transition-state structures for (a) [2$_s$ + 2$_a$] cycloreversion of malonic anhydrides and (b) [2$_s$ + (2$_s$ + 2$_s$)] cycloreversion of malonic anhydrides, with atomic-orbital overlaps indicated by wavy lines.

Notice that bonding to the C=C double bond of the ketene is to the + lobe of one atomic orbital and to the − lobe of the other, so this serves as the antarafacial component,[18] while the O=C of the CO$_2$ is the suprafacial component, with bonding to the atomic orbitals projecting forward toward the ketene. This corresponds to a Möbius topology for the cycle of atomic orbitals.[19] An alternative is a [2$_s$ + (2$_s$ + 2$_s$)] process,[20] with a cycle of six atomic orbitals that avoids an antarafacial component by using two p orbitals on the central carbon of the ketene. This is illustrated in Figure 1b, with the vertical p orbitals forming the C−C π bond and with the front lobe of the horizontal carbon p orbital in the ketene plane overlapping with the vertical orbital on a CO$_2$ oxygen. To achieve this overlap, this transition-state structure too must be twisted around the vertical C−C bond that is breaking simultaneously with the breaking of the vertical C−O bond.

We now report the first measurements of rate constants and activation parameters for decomposition of malonic anhydrides **2**, including those of the monomethyl derivative (**2b**, R = H, R′ = CH$_3$). The experimental data are reinforced by computations. The results provide definitive answers to the questions above regarding the rapidity of decomposition and the substituent effects on reactivities.

■ EXPERIMENTAL SECTION

Materials. Diketene (**1a**, Aldrich) was redistilled. The other two ketene dimers, 4-ethylidene-3-methyl-2-oxetanone (**1b**) and 3-hydroxy-2,2,4-trimethyl-3-pentenoic acid β-lactone (**1c**), were synthesized by established procedures.[21] Other reagents were obtained from commercial suppliers and used as received. Malonic (**2a**), methylmalonic (**2b**), and dimethylmalonic (**2c**) anhydrides were then produced by ozonolysis of the three ketene dimers.[7] Details are available.[22]

Sample Preparation. Solutions for ozonolysis were prepared in 200 μL of CDCl$_3$ in an NMR tube, to contain approximately 0.2 M diketene **1a**, 0.02 M methylketene dimer **1b**, or 0.1 M dimethylketene dimer **1c**, along with 0.02 M cyclopentane (δ 1.51), 0.02 M acetonitrile (δ 2.10), or 0.2 M acetonitrile, respectively, as internal standard. To scavenge peroxides, 1 or 0.1 M propionaldehyde (**6**) was included in the solution of **1a** or **1b**, respectively. Addition of **6** to scavenge dissolved peroxide dimers and trimers in the samples of **1b** or **1c** did not affect the kinetics. A combination sample of 0.1 M **1b**, 0.05 M **1c**, 0.2 M **6**, and 0.1 M acetonitrile was also prepared by use of a different distillation fraction of **1b** that contained more propionic

anhydride byproduct, in order to test whether this anhydride interferes with the kinetic experiments. It does not.

Ozonolysis. The sample was placed in a dry ice/acetone cooling bath, and ozonolysis by use of an Ozone Research and Equipment Corp. model 03 V5-O ozone generator was performed at −65 °C. Ozone gas was bubbled through the sample until the solution turned light blue, at which point O$_2$ was bubbled through to remove excess ozone. After ozonolysis, additional chilled CDCl$_3$ was added into the NMR tube so that the total sample volume was 600−700 μL.

Peroxide solids in the sample of **2a** were found to affect the rate of decomposition. Reproducible rates were obtained only after the peroxides were filtered off by quickly pouring the sample through a precooled 2-mL pipet tip equipped with a plug of cotton and pushing the liquid through the filter with N$_2$ pressure. Filtration had been also found applicable to the purification of acetic formic anhydride, formed by ozonolysis of vinyl acetate.[23] Peroxide solids in the samples of **2b** and **2c** were found not to interfere with the kinetics, because the results were the same regardless of filtering. Therefore those peroxides were not removed. Finally, the NMR tube was capped and the sample was frozen to permit transfer into the probe of the magnet. *Caution*: Peroxides are potentially explosive, especially as solids and in larger quantities than here. It might be mentioned that this study awaited instrumentation sensitive enough to measure kinetics safely at low concentrations.

NMR Measurements. All ^{1}H NMR spectra were acquired on a JEOL 500-MHz ECA spectrometer. For **2a** and **2b**, a tip angle of 68° and four acquisitions were used, with a repetition time of 6−8 s, sufficient for T_1 relaxation, which was measured independently for anhydrides and internal standards. For **2c**, a tip angle of 90° was used with a single acquisition. The free-induction decays were zero-filled (4×) to increase digital resolution, and line broadening of 0.2 Hz was applied. The spectra were processed with JEOL Delta and iNMR software. For each run the integration region was chosen by overlaying the spectra so that all the peaks would be integrated over the same region.

Temperature Adjustment. Prior to the experiment, the temperature of the probe was set in the Delta software. The probe was first set to −50 °C, and 15−20 min was allowed for cooling. Once the sample was inserted into the magnet, one spectrum was taken at −50 °C and then the temperature was set to the desired value. The sample was allowed to remain in the probe for 5 min to allow for temperature equilibration, and then the kinetic experiment began. The temperature inside the NMR probe was measured both before and after the run from the separation between the OH and CH$_3$ chemical shifts of an external 4% methanol in methanol-d_4 standard.[24] The change in temperature from before the run to after was considered to be the maximum variation in temperature during the run. That variation was found to be less than 1 °C for all runs.

Characterization of Products. Malonic anhydride (**2a**): ^{1}H NMR 4.1 ppm (s) (lit.[7] 4.1 ppm) and peroxides 5.0−6.0 ppm (lit.[7] 5.0−6.0 ppm). Decomposition product ketene monomer (**5a**) was observed at 2.3 ppm (s, 2H). Methylmalonic anhydride (**2b**): ^{1}H NMR 4.30 ppm (q, 1H, J = 8.0 Hz), 1.65 ppm (d, 3H, J = 8.0 Hz), and peroxides 1.0−2.0 and 5.0−6.0 ppm. Decomposition product methylketene (**5b**) was observed at 2.72 ppm (q, 1H, J = 7.3 Hz) and 1.69 ppm (d, 3H, J = 7.3 Hz). Dimethylmalonic anhydride (**2c**): ^{1}H NMR 1.63 ppm (s) (lit.[7] 1.5 ppm) and acetone peroxides 1.0−2.0 ppm. Decomposition product dimethylketene (**5c**) was observed at 1.69 ppm (s).

Ketene formation was never quantitative. All three ketenes (**5abc**) undergo hydrolysis or possibly polymerization during the course of the kinetic experiment. NMR signals that can be assigned to hydrolysis products of **5a** were at 2.1 and 2.2 ppm, corresponding to acetic acid and anhydride. Signals at 2.7 ppm and 1.02 ppm, corresponding to isobutyric acid or anhydride (lit.[25] 2.66 and 1.24 ppm), were observed from **5c**. Signals attributable to propionic acid or anhydride from hydrolysis of **5b** were not observed, presumably because they were obscured by the added propionaldehyde (**6**).

Kinetic Measurements. The time dependence of integrated signal intensities was measured at 5 °C intervals between 0 and 25 °C for **2a**,

between −10 and 15 °C for **2b**, and between 5 and 30 °C for **2c**. Time intervals between acquisitions were adjusted so that a minimum of 15 spectra were acquired per run, and so that the reaction was monitored for more than one half-life. Also, one decomposition reaction for each anhydride was monitored for >10 half-lives to determine whether any residual peaks were obscured by the anhydride signal.

Possible Interferences. Small residual signals near the chemical shift of **2c** were detected after the signal of **2c** had disappeared. These signals were assigned as peroxides, whose signals were also found in that region. Although these signals could erroneously augment the anhydride signal, the nonlinear analysis described below corrects for this, and the errors in the measured rate constants for **2c** are not larger than the errors for the other two samples, where no such interference was seen.

Even though water and chloroform are immiscible, trace water might hydrolyze an anhydride and deceptively increase the rate of its disappearance. To test this, the reaction of water with malonic anhydride (**2a**) was simulated by adding 2 equiv of ethanol to a sample of **2a** at −65 °C, immediately inserting it into the NMR probe cooled to −10 °C, and monitoring the subsequent reaction. As expected, the anhydride disappeared rapidly, with the immediate formation of ^{1}H NMR peaks at 1.31 ppm (t, 3H), 3.43 ppm (s, 2H), and 4.24 ppm (q, 2H), which are assigned to 3-ethoxy-3-oxopropanoic acid (monoethyl malonate), along with other signals at 2.1 ppm (s) and 4.11 ppm (q), which may be assigned to ethyl acetate from reaction of ketene **5a**. Inasmuch as malonic acid was not detected among any of our products, we conclude that residual water does not interfere with our kinetic experiments.

Data Analysis. At each time point the concentration of anhydride, A, normalized to the (constant) concentration of the standard, was obtained by dividing the integrated peak area of the anhydride by the integrated peak area of the standard. The first-order rate constant k for disappearance of the anhydride was then obtained by two methods. First, k was obtained from the slope of the linear plot of $\ln A$ versus time t (eq 1), which also gives σ, the standard error of that slope. Second, k was obtained by nonlinear regression analysis (Solver routine in an Excel spreadsheet) to fit the data to eq 2, where estimates for the initial concentration A_0 and the rate constant k were obtained from the fit to eq 1, and the residual intensity A_∞ was estimated as the intensity at the final time point. The term A_∞ accounts for any extraneous signals hidden under the anhydride peak, which might be seen at the end of the reaction. Nonlinear regression analysis also has the advantage of eliminating error caused by heteroskedasticity (time-dependent variance), arising from the increased error of the logarithm of a diminishing concentration. To distinguish these two rate constants, they will be designated as k_{lin} and k_{NL}, respectively.

$$\ln A = \ln A_0 - kt \qquad (1)$$

$$A = (A_0 - A_\infty)\exp(-kt) + A_\infty \qquad (2)$$

For each anhydride, activation parameters $\Delta H^\ddagger$ and $\Delta S^\ddagger$ (enthalpy and entropy of activation), as well as the standard errors in these quantities, were then obtained from a plot of $\ln(k_{lin}/T)$ or $\ln(k_{NL}/T)$ versus $1/T$ (eq 3, where T = absolute temperature, k_B = Boltzmann's constant, h = Planck's constant, and R = gas constant), which has a slope of $-\Delta H^\ddagger/R$ and an intercept of $\ln(k_B/h) + \Delta S^\ddagger/R$.

$$\ln(k/T) = \ln(k_B/h) + \Delta S^\ddagger/R - \Delta H^\ddagger/RT \qquad (3)$$

Computational Methods. All calculations were carried out on a Dell Optiplex PC with Intel Core 2 Duo processor. Structures of malonic anhydride (**2a**), ketene (**5a**), and CO_2 were built by use of GaussView 4.1.2 (Gaussian, Inc.) and optimized with the Gaussian03W program.[26] An initial transition-state structure was calculated at the HF/6-31G(d) level via the synchronous transit-guided quasi-Newton (STQN) method and the QST2 option. The validity of the transition-state structure was verified by calculating frequencies and reaction-path following along the intrinsic reaction coordinate (IRC). Geometry optimizations of reactants and products were next performed at the MP2/6-31G(d) level. The transition-state structure

was found by the STQN method and the QST3 option, with the transition-state structure obtained from the Hartree−Fock (HF) method as the initial guess. IRC calculations were then performed by use of the Möller−Plesset second-order (MP2) transition-state structure. Vibrational frequencies were calculated for each structure, and the zero-point energy (ZPE) was included in the total energy. No correction was applied for scaling factors,[27] because they affect total energies by <1 kcal/mol and relative energies by <0.1 kcal/mol. No correction was applied for basis-set superposition error.

To obtain more accurate energies, calculations at the MP2/cc-pVDZ, MP2/aug-cc-pVDZ (which was found suitable for modeling [2 + 2] cycloadditions involving allene, ketene, and other X=C=Y),[28] B3LYP/6-31G(d), B3LYP/cc-pVTZ, BPW91/6-31G(d), BPW91/6-311+G(3df,2p), B3LYP/6-311+G(3df,2p), and G3 levels were also done. Transition-state structures were calculated by use of the QST3 option, except for G3. Some of these calculations were also performed for the methyl and dimethyl analogues. Optimization of the transition structure by MP2/cc-pVTZ, MP2/cc-pVQZ, or B3LYP/cc-pVQZ was unsuccessful.

In addition to the above closed-shell calculations, unrestricted MP2, B3LYP, and BPW91 calculations using the 6-31G(d), cc-pVDZ, or 6-311+G(3df,2p) basis set and the QST3 option were performed to search for other transition-state structures. The UBPW91 method seems to be adequate for diradicals.[29] Larger basis sets, 6-311++G(2d,2p) and cc-pVTZ, did not converge. The possibility of a stepwise mechanism was tested further by breaking the C−O bond of the malonic anhydride ring and optimizing the structure. A QST3 calculation with UB3LYP/6-31G(d), BPW91/6-31G(d), or UBPW91/6-31G(d) gave a transition structure similar to that obtained by the UMP2/6-31G(d) calculation. Unrestricted calculations (UB3LYP) with larger basis sets such as cc-pVTZ and 6-311++G(2d,2p) failed to converge.

Finally, the effect of solvation was tested at the B3LYP/6-31G(d), UBPW916-31G(d), and UBPW91/6-311+G(3df,2p) levels by use of the polarizable continuum model (PCM) with chloroform (ε = 4.90) as solvent, but only the first two converged.

■ RESULTS

Rates of Decomposition of Malonic Anhydrides. The first-order rate constants k_{lin}, determined from logarithmic plots (eq 1), and k_{NL}, from nonlinear regression analysis (eq 2), for the decomposition of all three anhydrides **2abc** at each temperature can be found in Tables 1, 2, and 3. The tabulated

Table 1. Parameters from Nonlinear Fits for Decomposition of 2a at Various Temperatures

T (°C)	$10^4 k_{lin}$ (s^{-1})	$10^4 \sigma_{lin}$ (s^{-1})	% σ_{lin}	r	$10^4 k_{NL}$ (s^{-1})	$100(A_\infty/A_0)$
25.9	18.1	0.2	1.1	0.9990	18.0	0.007
20.7	10.1	0.1	1.4	0.9976	10.2	0.017
20.5	9.3	0.2	2.0	0.9939	9.3	0.022
15.7	6.70	0.08	1.1	0.9979	6.76	0.001
10.7	4.49	0.05	1.2	0.9975	4.42	−0.102
5.8	2.79	0.05	1.9	0.9960	2.85	0.067
0.8	1.73	0.01	0.8	0.9988	1.73	0.008
0.8	1.63	0.02	1.1	0.9978	1.61	0.018

values show only significant figures, but insignificant figures were retained for further calculations. Tables 1−3 also list σ_{lin} (the standard error in k_{lin}), % σ_{lin} (percent relative error of k_{lin}), r (correlation coefficient of the linear fit), and $100(A_\infty/A_0)$ (percent infinity absorbance not due to anhydride, determined from the nonlinear fit).

The logarithmic fits all give correlation coefficients r > 0.99, reflecting good linearity in the fit to eq 1. Therefore these reactions indeed follow first-order kinetics, with no indication

Table 2. Parameters from Nonlinear Fits for Decomposition of 2b at Various Temperatures

T (°C)	$10^4 k_{lin}$ (s⁻¹)	$10^4 \sigma_{lin}$ (s⁻¹)	% σ_{lin}	r	$10^4 k_{NL}$ (s⁻¹)	$100(A_\infty/A_0)$
15.6	14.08	0.07	0.5	0.9997	14.15	0.005
10.6	8.34	0.03	0.3	0.9999	8.21	0.003
10.6	7.38	0.17	2.4	0.9958	7.42	0.009
10.6	7.38	0.19	2.6	0.9938	7.63	0.009
10.7	8.32	0.03	0.4	0.9998	8.37	0.003
10.7	8.04	0.05	0.7	0.9997	7.73	0.003
10.7	7.14	0.08	1.2	0.9985	7.21	0.007
5.7	5.24	0.04	0.8	0.9993	5.18	0.002
0.8	3.51	0.03	0.9	0.9988	3.45	0.003
−3.8	2.29	0.04	1.6	0.9960	2.29	0.001
−9.1	1.43	0.01	0.9	0.9988	1.29	0.003

Table 3. Parameters from Nonlinear Fits for Decomposition of 2c at Various Temperatures

T (°C)	$10^4 k_{lin}$ (s⁻¹)	$10^4 \sigma_{lin}$ (s⁻¹)	% σ_{lin}	r	$10^4 k_{NL}$ (s⁻¹)	$100(A_\infty/A_0)$
31.4	11.15	0.04	0.4	0.9999	12.33	5.7
26.0	7.11	0.04	0.5	0.9998	7.86	3.8
20.9	4.54	0.01	0.3	0.9999	4.89	2.9
15.6	2.614	0.008	0.3	0.9999	2.78	3.2
15.6	2.671	0.009	0.3	0.9999	2.797	2.7
15.6	2.621	0.014	0.5	0.9998	2.981	7.0
10.6	1.476	0.014	0.9	0.9992	1.697	6.8
5.6	0.891	0.006	0.6	0.9994	1.036	6.5

of a second-order component that could be ascribed to dimerization or to reaction with the peroxide byproduct. The logarithmic fits give rate constants with an average relative error of 1%, which is excellent precision. The nonlinear fits give values of $100(A_\infty/A_0)$ for **2a** and **2b** very close to zero, corresponding to "complete" disappearance of the signals of these two anhydrides. However, the average value of $100(A_\infty/A_0)$ for **2c** corresponds to a residual signal intensity of 5% of the initial anhydride intensity. These infinity values agree well with the spectra, where no residual signal was observed for **2a** and **2b** but small residual peaks were observed in the spectrum of **2c**. Nevertheless, those residual signals in the sample of **2c** do not lead to an increase in the relative error % σ_{lin}, which is no worse than the error for **2a** and **2b**. Moreover, the nonlinear fit compensates for this residual intensity.

For all three anhydrides, the values of k_{NL} are more reliable because they account for both residual absorbance and heteroskedasticity. Errors in k_{lin} and k_{NL} are compared below.

The rate constants in Tables 1−3 confirm the previous qualitative observations that malonic anhydrides **2a** and **2c** decompose near or below room temperature, as does **2b**. Decomposition is fastest for methylmalonic anhydride (**2b**) and slowest for dimethylmalonic anhydride (**2c**). This nonlinear dependence on the number of methyl groups is a puzzle parallel to the lower reactivity of **2c** that was noted originally.

Activation Parameters. Figures 2 and 3 show plots of ln (k/T) versus $1/T$ for rate constants k_{lin} from logarithmic fits and for rate constants k_{NL} from nonlinear fits, respectively, for all three anhydrides **2abc**. The two plots appear very similar. The slopes, standard errors of the slope, intercepts, standard errors of the intercepts, correlation coefficients, and standard error of the y estimate ($\sigma_{\ln k}$) found from these plots are listed in Table 4. The values hardly differ between linear and
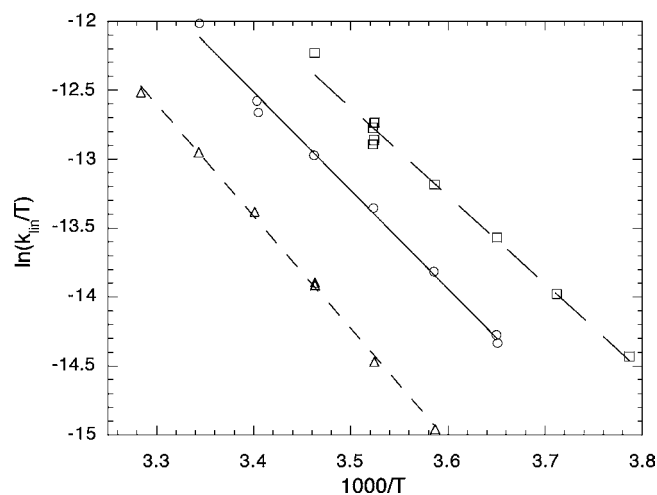
Figure 2. Eyring plot for anhydrides **2abc** from the rate constants from linear fits: (○) parent, (□) methyl, and (△) dimethyl.
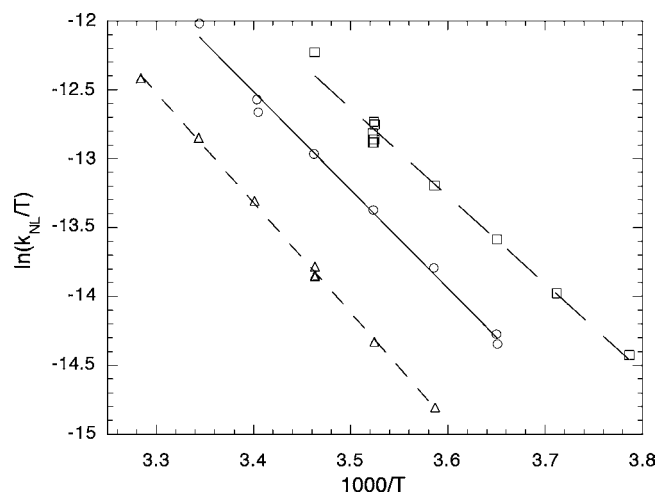
Figure 3. Eyring plot for anhydrides **2abc** from the rate constants from nonlinear fits: (○) parent, (□) methyl, and (△) dimethyl.

Table 4. Slope, Intercept, Correlation Coefficient, and Standard Error of y for Plots in Figures 2 and 3

anhydride	fit	slope	intercept	r	σ_{lnk}
2a	lin	−7.1 ± 0.2	11.7 ± 0.8	0.9972	0.068
2a	NL	−7.1 ± 0.2	11.7 ± 0.8	0.9972	0.068
2b	lin	−6.4 ± 0.3	9.7 ± 0.9	0.9928	0.080
2b	NL	−6.6 ± 0.2	10.6 ± 0.9	0.9941	0.075
2c	lin	−8.1 ± 0.1	14.2 ± 0.5	0.9991	0.037
2c	NL	−8.0 ± 0.1	13.8 ± 0.4	0.9994	0.028

nonlinear fits. The correlation coefficients found from these plots are all >0.99. The activation parameters $\Delta H^{\ddagger}$ and $\Delta S^{\ddagger}$ for each anhydride were determined from the slopes and intercepts of those plots. Insofar as the plots are adequately linear, there is no evidence that $\Delta H^{\ddagger}$ is temperature-dependent or that there is any detectable $\Delta C_p^{\ddagger}$. The values, along with their errors, are listed in Table 5.

Error Analysis. Errors in the rate constants were determined by three different methods. The first was σ_{lin}, from the error in the slope of the logarithmic plots, as listed in Tables 1−3. The second method was from $\sigma_{\ln k}$, the standard deviation of the y estimate in Table 4. Because this could be

Table 5. Enthalpy and Entropy of Activation for Anhydrides 2abc from Linear and Nonlinear Fits

anhydride	fit	$\Delta H^{\ddagger}$ (kcal/mol)	$\Delta S^{\ddagger}$ [cal/(mol·K)]
2a	lin	14.2 ± 0.4	−24.0 ± 1.5
2a	NL	14.2 ± 0.4	−23.9 ± 1.5
2b	lin	12.7 ± 0.5	−27.9 ± 1.8
2b	NL	12.6 ± 0.5	−28.1 ± 1.7
2c	lin	16.2 ± 0.3	−18.9 ± 1.0
2c	NL	15.9 ± 0.2	−19.8 ± 0.8

converted to σ_k as in eq 4, it represents the relative error in the rate constant. Multiplying this by 100 gives the percent error in k, designated as % σ_k. Thus the values of % σ_k for the linear fits are 6.8%, 8.0%, and 3.7% for **2a**, **2b**, and **2c**, respectively, and 6.8%, 7.5%, and 2.8% for the nonlinear fits. Because the relative errors from the nonlinear fits are slightly smaller, they are confirmed to be more reliable.

$$\sigma_{\ln k} = (\partial \ln k/\partial k)\sigma_k = (1/k)\sigma_k \qquad (4)$$

The third measure of the error in the rate constants is the variation between experiments repeated at the same temperature. These repetitions are included in Tables 1−3 and in Figures 2 and 3. They are summarized in Table S1 in Supporting Information, expressed as % σ_k^T, the percent deviation of rate constant at that temperature, from linear and nonlinear fitting. The values of % σ_k^T are comparable to the percentage errors in k or to $\sigma_{\ln k}$ in Table 4. However, the latter errors are more reliable because they are determined from more data points.

It should be noted that the error % σ_{lin} in Tables 1−3 is the smallest of all error estimates, because it is a within-run error, rather than a run-to-run error. The value % σ_{lin} includes error due to the variation in temperature during a single experiment, whereas the value % σ_k from Table 4 includes error due to the variation in temperature from run to run. The contribution due to this variation is given in eq 5, where the first term is negligible compared to the second. The uncertainty, σ_T, previously reported as ±0.8 K,[30] is entirely consistent with the observed % σ_k. Therefore we conclude that the major source of errors in the rate constants is due to imperfect control of temperature, but those errors are small. Moreover, the errors in $\Delta H^{\ddagger}$ and $\Delta S^{\ddagger}$ in Table 5 are realistic estimates.

$$\sigma_{\ln k} = (\partial \ln k/\partial T)\sigma_T = (1/T + \Delta H^{\ddagger}/RT^2)\sigma_T \qquad (5)$$

Summary of Kinetics Experiments. These experimental results confirm and quantify the previous observation[7] that **2a** decomposes faster than **2c**. Moreover, we find that **2b** decomposes even faster than either **2a** or **2c**. This can be seen by comparing data in Tables 1−3 at similar temperatures or more explicitly from rate constants $(6.4 \pm 0.4) \times 10^{-4}$ s^{-1} for **2a**, $(11.3 \pm 0.9) \times 10^{-4}$ s^{-1} for **2b**, and $(2.7 \pm 0.1) \times 10^{-4}$ s^{-1} for **2c**, interpolated at 15.0 °C from Figure 3. Alternatively, these rate constants correspond to values of $\Delta G^{\ddagger}$ of 21.06 ± 0.04 kcal/mol for **2a**, 20.73 ± 0.05 kcal/mol for **2b**, and 21.55 ± 0.02 kcal/mol for **2c**. Parallel to the rate constants, **2b** shows a $\Delta G^{\ddagger}$ value significantly lower than those of the other two anhydrides.

According to the data in Table 5, $\Delta H^{\ddagger}$ is highest for **2c** and lowest for **2b**. This result reinforces the nonlinear dependence of the rate constants on the number of methyl groups. The entropy of activation is least negative for **2c** and is most negative for **2b**, although the difference between **2b** and **2a** is

barely significant at a 95% confidence level. Indeed, an apparent compensation between enthalpy and entropy is often an artifact of experimental error.[31]

Computational Results. Calculated energies for each of the species, by the various computational methods, are listed in Table S2 in Supporting Information. All reactants and products are minima, with no imaginary frequencies, whereas the transition states have one imaginary frequency. It may be noted that the four atoms of the malonic anhydride ring are not coplanar, although the barrier to ring inversion is too small to calculate. Energies of the transition state and of the products, ketene (**5a**) + CO$_2$, relative to the reactant malonic anhydride (**2a**), are summarized in Table 6. Table 7 presents these values for methylmalonic (**2b**) and dimethylmalonic (**2c**) anhydrides.

Table 6. Calculated Energies of Transition State and Product, Relative to Malonic Anhydride

method	$E_{\text{rel}}^{\ddagger}$ (kcal/mol)	$E_{\text{rel,pdt}}$ (kcal/mol)
HF/6-31G(d)[a]	39.16	−4.32
MP2/6-31G(d)[a]	33.45	−1.07
MP2/6-31G(d)	31.06	−5.13
MP2/cc-pVDZ	28.84	−9.60
MP2/aug-cc-pVDZ	26.55	−5.96
UB3LYP/6-31G(d)	29.71[b]	−3.89
B3LYP/6-31G(d)[c]	25.88	
B3LYP/cc-pVTZ	26.28	−11.86
B3LYP/6-311+G(3df,2p)	25.75	−11.85
UBPW91/6-31G(d)	26.05[b]	−2.95
UBPW91/6-31G(d)[c]	23.88	
UBPW91/6-311+G(3df,2p)	22.98[b]	−9.46
G3		−4.61

[a]Uncorrected for zero-point energies. [b]Same with restricted. [c]PCM (solvent = chloroform).

Table 7. Calculated Energies of Transition State and Product, Relative to Methylmalonic or Dimethylmalonic Anhydride

method	$E_{\text{rel}}^{\ddagger}$ (kcal/mol)	$E_{\text{rel,pdt}}$ (kcal/mol)
Relative to Methylmalonic Anhydride (**2b**)		
B3LYP/6-31G(d)	28.30	−1.43
B3LYP/cc-pVTZ	25.19	−8.80
B3LYP/6-311+G(3df,2p)	24.80	−8.64
G3		−0.40
Relative to Dimethylmalonic Anhydride (**2c**)		
B3LYP/6-31G(d)	29.86	−0.29
B3LYP/cc-pVTZ	27.19	−7.18
B3LYP/6-311+G(3df,2p)	26.79	−6.86
G3		3.08

■ DISCUSSION

Computed Exothermicity. As starting points, the decomposition of malonic anhydride (**2a**) was calculated at the HF/6-31G(d) level without ZPE correction and at MP2/6-31G(d) including ZPE. According to the results in Table 6, an exothermicity of 4.3 or 5 kcal/mol is obtained.

According to the MP2/cc-pVDZ and MP2/aug-cc-pVDZ calculations, the exothermicity is 10 and 6 kcal/mol, respectively. The exothermicity obtained at the B3LYP/6-31G(d) level is 4 kcal/mol, comparable to that at MP2/6-31G(d). According to the B3LYP/cc-pVTZ, B3LYP/6-311+G-

(3df,2p), and BPW91/6-311+G(3df,2p) calculations, the exothermicity is increased, approaching 12 kcal/mol. According to the G3 method, which generally gives enthalpies of formation accurate to ±1 kcal/mol,[32] the exothermicity is only 4.6 kcal/mol. However, Table S2 (Supporting Information) shows that the B3LYP/6-31G(d), B3LYP/cc-pVTZ, B3LYP/6-311+G(3df,2p), and BPW91/6-311+G(3df,2p) absolute energies for **2a**, ketene, and CO_2 are all more negative than the G3 energies. Therefore, by the variation principle of quantum mechanics,[33] the G3 energies are not sufficiently reliable for this study. We therefore accept a calculated value of 10−12 kcal/mol for the exothermicity of conversion of **2a** to **5a** + CO_2.

Computed Activation Energy. According to the result in Table 6, an activation energy of 39 kcal/mol is obtained at the HF/6-31G(d) level without ZPE correction. The resulting transition-state structure has all the heavy atoms lying in essentially the same plane but with an increased separation between the atoms involved in bond breaking. Electron correlation is known to be especially significant in transition states,[34] as confirmed by the MP2/6-31G(d) calculations, which predict an activation energy ∼6 kcal/mol lower than that of the HF method. Inclusion of ZPE corrections leads to a slight further lowering of the activation energy.

The importance of electron correlation becomes more apparent when the calculated transition-state structures are compared. Whereas a planar structure was calculated by the HF method, a twisted transition-state structure (Figure 4) was
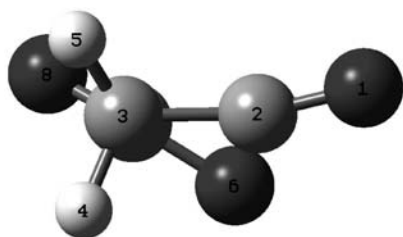

Figure 4. Transition-state structure for thermal decomposition of malonic anhydride, as calculated at the MP2/6-31G(d) level.

found by the MP2 calculation. The OCCC dihedral angle is 32°. This twisting is much less than in Figure 1a, where the twisting is exaggerated in order to depict the atomic-orbital overlaps. Figure 5 shows the framework and two contours of the highest occupied molecular orbital of the B3LYP6-31G(d) transition state. Atomic orbitals on all six atoms are involved, including both oxygens of CO_2 and also including two p

orbitals on the central carbon of the ketene. This is consistent with a $[2_s + (2_s + 2_s)]$ process, but the interaction of one C=O of CO_2 with the C=C of ketene is antarafacial, which is consistent with a $[2_s + 2_a]$ process. Although this process was rejected for the dimerization of ketene,[35] we choose not to distinguish between them.

According to the MP2/cc-pVDZ and B3LYP/6-31G(d) calculations, the activation energy is 29 and 30 kcal/mol, respectively, or slightly lower, ∼26 kcal/mol, by MP2/aug-cc-pVDZ, B3LYP/cc-pVTZ, and B3LYP/6-311+G(3df,2p) methods and 23 kcal/mol by BPW91/6-311+G(3df,2p). The transition-state structures look similar in all cases and also similar to that in Figure 4 or 5 but with an OCCC dihedral angle of 27°.

The possibility of a stepwise mechanism was also explored by using the unrestricted UMP2/6-31G(d), UB3LYP/6-31G(d), UBPW91/6-31G(d), and UBPW91/6-311+G(3df,2p) methods, which allow for a stepwise mechanism, but the calculated activation energies are unchanged. Moreover, the transition-state structures are virtually identical to those obtained by the corresponding restricted methods.

The possibility of a stepwise mechanism was further explored by searching for reaction intermediates, but this calculation converged only to the optimized malonic anhydride structure. In another calculation, the CO_2 moiety was twisted by 90° after breaking the C−O bond of the ring. Geometry optimization of this structure did not reach a minimum. For another attempt at geometry optimization to a stable intermediate, the C−C bond parallel to the C−O bond of the ring was broken instead, but this calculation led to the optimized malonic anhydride structure. Similar results were obtained for the calculations in the presence of a solvent continuum. Thus, no reaction intermediates were found. We therefore conclude that the reaction is concerted, not stepwise.

According to the BPW91/6-311+G(3df,2p) calculations, the C−C bond that is being broken has elongated from 1.524 Å in **2a** to 1.780 Å in the transition-state structure, while the C−O bond that is being broken has elongated from 1.426 to 2.130 Å, in part because of the twisting of the OCCC dihedral angle by 30°. Therefore, although this is a concerted process, it is quite asynchronous, with C−O cleavage occurring in advance of C−C cleavage. However, in contrast to the cycloaddition of alkenes with isocyanates, for which the transition-state structure is zwitterionic,[36] the B3LYP/6-311+g(3df,2p) Mulliken charges show a $C^{\delta^+}-O^{\delta^-}$ character smaller than in the anhydride, whereas the UBPW91/6-311+G(3df,2p) charges show a
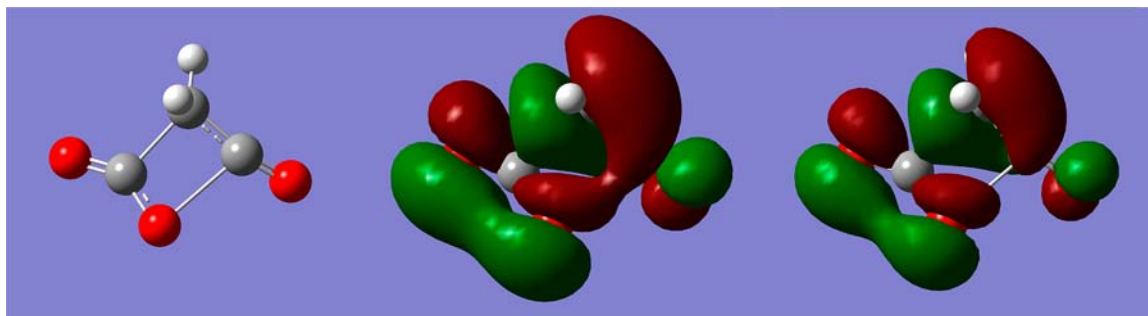

Figure 5. Atomic framework and two contours of the highest occupied molecular orbital of the transition-state structure for decomposition of malonic anhydride, as calculated at the B3LYP/6-31G(d) level.

greater $O^{\delta-}$ character in the transition-state structure than in the anhydride but a smaller $C^{\delta+}$ character.

The above calculations ignore solvation. The importance of solvation is demonstrated by the B3LYP/6-311+G(3df,2p) calculation that shows that the dipole moment of the transition-state structure is 5.26 D, appreciably larger than the 2.91 D of the reactant **2a**. Therefore, a polar solvent is likely to accelerate the reaction. Such solvation can be taken into consideration by PCM simulation, with chloroform as solvent. Then the activation energy calculated by the B3LYP/6-31G(d) method drops from 29.7 to 25.9 kcal/mol, or from 26.05 to 23.9 kcal/mol with UBPW91/6-31G(d), a decrease of 2−4 kcal/mol.

Experimental Enthalpy of Activation. As can be seen from Table 5, the experimentally measured $\Delta H^{\ddagger}$ is quite low: 14.2 ± 0.4, 12.6 ± 0.5, or 15.9 ± 0.2 kcal/mol for the thermal decomposition of **2a**, **2b**, or **2c**, respectively. Low values are consistent with a concerted cycloreversion, where a stabilization due to bond formation compensates for the energy rise due to bond breaking. In contrast, for a representative stepwise process, the decomposition of cyclobutane, the activation enthalpy is much higher, 61 kcal/mol experimentally or 63 kcal/mol computationally.[37] Lower activation enthalpies, 27.5 and 48 kcal/mol, are found for two concerted cycloreversions of dicyclopentadiene and diketene, respectively.[38] Yet our observed values are considerably lower even than these. Indeed, the unusually low activation energy, or the correspondingly rapid decomposition, is the reason why malonic anhydrides eluded synthesis for so long.

The decomposition of malonic anhydrides must be concerted, without any intermediate diradical or zwitterion, because neither the C−O bond nor the C−C bond is so weak that the activation energy for its cleavage would be <16 kcal/mol. A concerted process is supported by the calculations that fail to find an intermediate. Thus we avoid the mechanistic uncertainty that has long plagued the study of cycloaddition and cycloreversion reactions.

One reason for the low activation energy is the exothermicity of the reaction, due to the stability of CO_2. According to the experimental ΔH_f° of CO_2 and of ketene (−393.5 and −47.5 kJ·mol^{-1})[39a] and the estimated ΔH_f° of malonic anhydride (−407 kJ·mol^{-1}),[5] the decomposition of malonic anhydride is exothermic by 8 kcal/mol (although this is an underestimate owing to comparison of malonic anhydride with reference four-membered-ring compounds that lack the carboxyls in the destabilizing anti conformation). This agrees quite well with our computational results of 10−12 kcal/mol at the B3LYP/cc-pVTZ, B3LYP/6-311+G(3df,2p), and BPW91/6-311+G-(3df,2p) levels.

Our computational results lead to an activation energy of 23−26 kcal/mol. This is a substantial overestimate relative to the experimental 13−16 kcal/mol. The discrepancy between these calculated activation energies and the experimental ones can be attributed largely to the neglect of solvation. When solvation by chloroform is taken into consideration with PCM, the activation energy calculated by the B3LYP/6-31G(d) or UBPW91/6-31G(d) method drops by 2−4 kcal/mol. If this decrease is applied to the activation energy calculated at the UBPW91/6-311+G(3df,2p) level (which did not converge with PCM), the activation energy is estimated to drop to 19−21 kcal/mol, which is still higher than the experimental value but not so much as to invalidate the calculations or the experiments. Because the activation energy has not reached a

limiting value even with cc-pVTZ or 6-311+G(3df,2p), it is possible that a larger basis set or an alternative methodology might give a lower value, as might a more accurate treatment of solvation, but such computations are unlikely to justify the effort when their chief purpose is to complement the experimental results.

Despite the discrepancy, both the calculated activation energy and the experimental values are much lower than for other cycloreversions. Indeed, most cycloreversions have quite high activation energies, because those reactions are so endothermic that they are usually studied in the direction of cycloaddition. The activation energy for cycloreversion is then the sum of the activation energy of cycloaddition and the reaction enthalpy. The closest analogue to a malonic anhydride is a malonimide (2,4-azetidinedione), which is prepared from a ketene and an isocyanate,[40] a reaction that is slightly exothermic,[41] or by cyclization of a malonic acid derivative,[42] and which does not decompose. One of the most studied classes of cycloadditions is of ketenes with imines, which proceeds stepwise but is not fully understood.[43] Similar is the cycloaddition of ketenes (or isocyanates) with aldehydes, but this is concerted.[44]

Yet exothermicity cannot be the only reason. For example, the decomposition of oxetanone (β-propiolactone) to ethylene + CO_2 is slightly more exothermic (12 kcal/mol).[45] Nevertheless, the activation energy for this decomposition is much higher, 45.8 kcal/mol.[46]

We suggest that the other reason for the low activation energy is the $[2_s + (2_s + 2_s)]$ or $[2_s + 2_a]$ nature of the reaction pathway. An sp-hybridized central C, as in the ketene product, is needed to provide two p orbitals for the cycle of six atomic orbitals or for the antarafacial component. In the (also exothermic) decomposition of oxetanone, only the carbon atom of CO_2 can provide two p orbitals for the cycle,[47] but the required twisting decreases the stabilization of CO_2 below what will be realized in the products.

Effects of Methyl Substitution. The remaining puzzle regarding $\Delta H^{\ddagger}$ for decomposition of malonic anhydrides is the nonlinear dependence on the number of methyl groups, with $\Delta H^{\ddagger}$ lowest for the monomethyl (**2b**) and highest for the dimethyl (**2c**). The lowest $\Delta H^{\ddagger}$ might have been expected for the latter, whose methyl groups could stabilize the C−C double bond forming in the transition-state structure.

However, the stabilization of ketenes by methyl substitution is much less than the stabilization of alkenes.[48] It is even doubtful whether there is any net stabilization by methyl of an sp^2 carbon in ketene. The calculated effect of one or two added methyls on ΔH_f° of ketene is −16 or −40 kJ·mol^{-1},[49] whereas the effect of one or two added methyls on ΔH_f° of ethane is −19.8 or −50.2 kJ·mol^{-1}.[39b] Therefore, a methyl group appears to *destabilize* the sp^2 carbon of ketene by ~4 kJ·mol^{-1} more than it does an sp^3 carbon.

The data in Tables 6 and 7 support this conclusion. According to the B3LYP/6-31G(d) calculations, the exothermicity decreases from 3.89 kcal/mol for **2a** to 1.43 and 0.29 kcal/mol for **2b** and **2c**. For the G3 calculations, which we consider less reliable, these values are 4.61, 0.40, and −3.08 (endothermic), respectively. For the more reliable B3LYP/cc-pVTZ calculations, the exothermicities are 11.86, 8.80, and 7.18 kcal/mol, respectively; and the values are 11.85, 8.64, and 6.86 kcal/mol for B3LYP/6-311+G(3df,2p). In short, methylation destabilizes the product ketene relative to the reactant anhydride.

Therefore, the methyls should not have been expected to accelerate the decomposition. Instead, the methyls retard decomposition through steric destabilization of the twisted transition-state structure (Figure 1b), which brings one of them closer to one of the oxygens of the CO_2. According to the B3LYP/cc-pVTZ calculation on the parent **2a**, the distances between an H and the oxygens of the CO_2 have shortened from 2.889 and 3.043 Å in the anhydride to 2.647 and 2.925 Å in the transition-state structure. For the dimethyl anhydride (**2c**), the distances between an H on each methyl and one or the other oxygen of CO_2 have shortened from >3.214 Å to 2.664 and 2.783 Å. For comparison, the sum of the van der Waals radii for hydrogen and oxygen is 2.72 Å.[50] A similar increase in $\Delta H^{\ddagger}$ due to steric repulsion was seen for $[2 + 2]$ cycloaddition of ethoxyketene to *cis*- versus *trans*-2-butene.[51]

The higher $\Delta H^{\ddagger}$ for **2c** is reproduced by the results in Tables 6 and 7. According to the more reliable B3LYP/cc-pVTZ calculations, the activation energies for **2a** and **2c** are 26.28 and 27.19 kcal/mol, respectively, or 25.75 and 26.79 kcal/mol according to B3LYP/6-311+G(3df,2p). The difference of 1 kcal/mol is small but consistent with the experimental difference of 1.7 ± 0.45 kcal/mol from Table 5.

Because **2c** has the highest $\Delta H^{\ddagger}$, steric effects are a dominant influence on the rates of decomposition of methyl-substituted malonic anhydrides. Yet if steric effects were the only influence, then the order of reactivity would be **2a** > **2b** > **2c**. Instead there is a nonlinear dependence of rate on the number of methyl groups, with **2b** faster than **2a**, and with a $\Delta H^{\ddagger}$ lower by 1.6 ± 0.6 kcal/mol, according to the data in Table 5. This is opposite to any steric effect. Of course, steric repulsion can be avoided, because the single methyl group of **2b** can project away from the CO_2, as does the R′ in the rear of Figure 1b.

The lower $\Delta H^{\ddagger}$ for **2b** represents a stabilization of its transition state. According to the calculated exothermicities, this is a stabilization that does not appear in the product. Yet this lower $\Delta H^{\ddagger}$ is reproduced by the results in Tables 6 and 7. According to the more reliable B3LYP/cc-pVTZ calculations, the activation energies for **2a** and **2b** are 26.28 and 25.19 kcal/mol, respectively, or 25.75 and 24.80 kcal/mol according to B3LYP/6-311+G(3df,2p). This difference of 1 kcal/mol is also small but consistent with the experimental difference of 1.6 ± 0.6 kcal/mol from Table 5.

What is the origin of this stabilization, which appears only in the transition state and not in the product? One possibility is hyperconjugation, whereby an electron-donating methyl stabilizes the delocalized electronic structure of the transition state. In support, the B3LYP/6-311+G(3df,2p) total charge on the methyl group in the transition-state structure **2b**‡ is +0.166, greater than the total charge either of +0.102 in reactant **2b** or of +0.049 in product methylketene (**5b**). Thus electron donation by the methyl is strongest in the transition state (although the effect is less marked with B3LYP/cc-pVTZ charges).

The increase in $\Delta\Delta H^{\ddagger}$ due to the steric destabilization of the transition-state structure by one methyl can be estimated. This is the difference between the experimental $\Delta H^{\ddagger}$ for **2c** and $\Delta H^{\ddagger}$ for **2b**, which lacks steric destabilization, but this difference must be corrected for the 1.6 ± 0.6 kcal/mol of stabilization in **2c** due to one extra methyl group. Thus the steric destabilization of the transition-state structure by one methyl group is 15.9 − 12.6 + (14.2 − 12.6) kcal/mol, or 4.9 ± 1.1 kcal/mol.

These estimates are plotted on an energy diagram in Figure 6, which shows the relative enthalpies of the transition-state
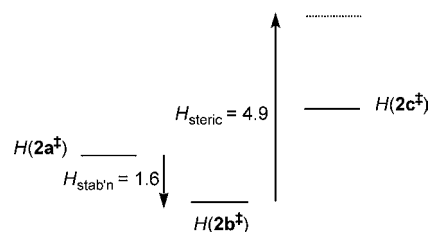

Figure 6. Relative transition-state enthalpies for decomposition of malonic anhydrides.

structures for decomposition of **2a**, **2b**, and **2c**. The dashed line for **2c** represents the enthalpy of the hypothetical transition-state structure without electronic stabilization by the two methyl groups. The figure also reproduces the observation that $\Delta H^{\ddagger}$ is not linear in the number of methyl groups. In summary, the reason why **2c** has the highest $\Delta H^{\ddagger}$ is that the steric retardation by the second methyl is greater than the stabilization of the delocalized electronic structure of the transition state by two methyls.

Entropy of Activation. As can be seen from Table 5, $\Delta S^{\ddagger}$ is substantially negative for decomposition of all three malonic anhydrides (**2abc**). This might be thought unusual for a decomposition that converts one molecule to two and where the overall $\Delta S° > 0$. However, a negative $\Delta S^{\ddagger}$ is also seen in the classic example of the decomposition of dicyclopentadiene.[52]

The negative $\Delta S^{\ddagger}$ is due to the necessity of organizing the structure to permit the orbital overlaps in the transition-state structure (Figures 1b, 4, and 5). The least negative is for **2c**. This may be a consequence of the steric repulsion, whereby the transition-state structure has a more pronounced character of fragmentation. The more interesting result is the 4.2 ± 2.3 cal/(mol·deg) more negative $\Delta S^{\ddagger}$ for **2b** than for **2a**. This is consistent with a contribution of $R \ln 2$, arising from the ability of **2a** to twist in two directions to reach the transition-state structure of Figure 1b or 4, whereas **2b** can twist in only one way to avoid methyl repulsion.

■ CONCLUSIONS

The rate constants and activation parameters for thermal decomposition of malonic anhydrides **2a**, **2b**, and **2c** were reliably obtained. The parent malonic anhydride **2a** was found to decompose at a higher rate than that of **2c**, and methylmalonic anhydride **2b** decomposes at an even higher rate than either **2a** or **2c**.

Computations support a twisted transition-state structure as illustrated in Figure 4 or 5. The low $\Delta H^{\ddagger}$ values provide additional evidence supporting a $[2_s + (2_s + 2_s)]$ or $[2_s + 2_a]$ cycloreversion mechanism, but they are exceptionally low, owing to the formation of the stable CO_2 product. The $\Delta H^{\ddagger}$ values increase in the order **2b** < **2a** < **2c**, owing to opposition between steric hindrance by a methyl group and its hyperconjugative ability to stabilize the delocalized transition-state structure, which is less effective.

The $\Delta S^{\ddagger}$ values for all three anhydrides are large and negative, consistent with a highly ordered transition-state structure, as predicted for $[2_s + (2_s + 2_s)]$ or $[2_s + 2_a]$ cycloreversions and as supported by calculations. The $\Delta S^{\ddagger}$ for

2a is less negative than that of **2b** because **2a** can twist in two different ways to reach the transition-state structure.

Despite the long-standing controversies and uncertainties regarding whether 2 + 2 cycloadditions and cycloreversions are concerted or stepwise, all these results are consistent with a concerted but asynchronous mechanism. The unusually low $\Delta H^{\ddagger}$ decisively excludes a stepwise process because there is no bond so weak that the activation energy for its cleavage would be <16 kcal/mol.

■ ASSOCIATED CONTENT

Ⓢ Supporting Information

Complete ref 26 and 63 tables, summarizing rate constants for decomposition of malonic anhydrides (**2abc**) from repeated runs at the same temperature; energies, as calculated by HF/6-31G, MP2/6-31G(d), MP2/cc-pVDZ, MP2/aug-cc-pVDZ, B3LYP/6-31G(d), B3LYP/cc-pVTZ, G3, B3LYP/6-311+G-(3df,2p), and UBPW91/6-311+G(3df,2p); and optimized geometries of malonic anhydride, ketene, CO_2, the transition-state structure, and their methyl and dimethyl analogues, as calculated by HF/6-31G, MP2/6-31G(d), MP2/cc-pVDZ, MP2/aug-cc-pVDZ, B3LYP/6-31G(d), B3LYP/cc-pVTZ, G3, B3LYP/6-311+G(3df,2p), and UBPW91/6-311+G(3df,2p). This material is available free of charge via the Internet at http://pubs.acs.org.

■ AUTHOR INFORMATION

Corresponding Author

cperrin@ucsd.edu

Present Address

[†]Institute of Chemistry, University of the Philippines Los Baños College, Laguna 4031, Philippines

Notes

■ ACKNOWLEDGMENTS

■ REFERENCES

(1) Cason, J. *Org. Synth.* **1963**, Collect. Vol. *IV*, p 630.
(2) Diels, O.; Wolf, B. *Chem. Ber.* **1906**, *39*, 689.
(3) Adam, W.; Diehl, J. W. *J. Chem. Soc., Chem. Commun.* **1972**, *13*, 797.
(4) (a) Einhorn, A.; von Dlesbach, H. *Chem. Ber.* **1906**, *39*, 1222. (b) Einhorn, A.; von Dlesbach, H. *Liebigs Ann.* **1908**, *359*, 145. (c) Staudinger, H.; Ott, E. *Chem. Ber.* **1908**, *41*, 2208. (d) Staudinger, H.; Ott, E. *Chem. Ber.* **1908**, *41*, 3829. (e) Duckworth, A. C. *J. Org. Chem.* **1962**, *27*, 3146. (f) Resofszki, G.; Huhn, M.; Hegedüs, B.; Dvortsák, P.; Kálóy, K. *Tetrahedron Lett.* **1975**, 3091.
(5) Perks, H. M.; Liebman, J. F. *Struct. Chem.* **2000**, *11*, 265.
(6) Jones, K. M.; Tomkinson, N. C. O. *J. Org. Chem.* **2012**, *77*, 921.
(7) Perrin, C. L.; Arrhenius, T. *J. Am. Chem. Soc.* **1978**, *100*, 5249.
(8) Schwartz, C.; Raible, J.; Mott, K.; Dussault, P. H. *Org. Lett.* **2006**, *8*, 3199.
(9) Keul, H.; Kuczkowski, R. L.; Choi, H.-S. *J. Org. Chem.* **1985**, *50*, 3365.
(10) Perrin, C. L.; Magde, D.; Berens, S. J.; Roqué, J. *J. Org. Chem.* **1980**, *45*, 1705.
(11) Even higher frequencies are seen in carbon monoxide and metal carbonyls, with C≡O character, and in X=Y=Z systems, such as ketenes, which vibrate as a three-atom unit. The only other organic carbonyl compound with such a high-frequency vibration as malonic anhydride is β,β-bis(trifluoromethyl)-β-propiolactone, whose stretching frequencies were claimed to be at 1890 and 1949 cm^{-1} (Knunyants, I. L.; Cheburkov, Yu. A. *Izv. Akad. Nauk SSSR, Ser. Khim.* **1960**, *678*, via CAN *54*, 117538), but this seems improbably high for a β-lactone, inasmuch as β-butyrolactone absorbs at 1823 cm^{-1}.
(12) Perrin, C. L. U.S. Patents 4,251,447, 1981, and 4,360,691, 1982.
(13) Some recent examples include the following: (a) Vaske, Y. S. M.; Mahoney, M. E.; Konopelski, J. P.; Rogow, D. L.; McDonald, W. J. *J. Am. Chem. Soc.* **2010**, *132*, 11379. (b) Yu, J.; Ding, W.; Lian, G.; Song, K.; Zhang, D.; Gao, X.; Yang, D. *J. Org. Chem.* **2010**, *75*, 3232. (c) Li, W.; Chen, Y.; Lam, Y. *Tetrahedron Lett.* **2004**, *45*, 6545.
(14) O'Murchu, C. *Eur. Pat. Appl.* EP 496362, 1992.
(15) Lipson, V. V.; Gorobet, N. Y. *Mol. Diversity* **2009**, *13*, 399.
(16) Lorencak, P.; Pommelet, J. C.; Chuche, J.; Wentrup, C. *J. Chem. Soc., Chem. Commun.* **1986**, *13*, 369.
(17) Anslyn, E. V.; Dougherty, D. A. *Modern Physical Organic Chemistry*; University Science Books: Sausalito, CA, 2006; p 588f.
(18) Woodward, R. B.; Hoffmann, R. *Angew. Chem., Int. Ed. Engl.* **1969**, *8*, 781.
(19) (a) Dewar, M. J. S. *Tetrahedron Suppl.* **1966**, *8*, 75. (b) Zimmerman, H. E. *Acc. Chem. Res.* **1971**, *4*, 272. (c) Perrin, C. L. *Chem. Br.* **1972**, *8*, 163.
(20) (a) Pasto, D. J. *J. Am. Chem. Soc.* **1979**, *101*, 37. (b) Valenti, E.; Pericas, M. A.; Moyano, M. *J. Org. Chem.* **1990**, *55*, 3582. (c) Seidl, E. T.; Schaefer, H. F., III. *J. Am. Chem. Soc.* **1991**, *113*, 5195.
(21) (a) Sauer, J. C. *J. Am. Chem. Soc.* **1947**, *69*, 2444. (b) Hasek, R. H.; Clark, D.; Elam, E. U.; Martin, J. C. *J. Org. Chem.* **1961**, *27*, 60.
(22) Flach, A. Ph.D. Thesis, University of California at San Diego, 2012.
(23) Lapalme, R.; Borschberg, H.-J.; Soucy, P.; Deslongchamps, P. *Can. J. Chem.* **1979**, *57*, 3272.
(24) Berger, S.; Braun, S. *200 and More NMR Experiments*; Wiley−VCH: Weinheim, Germany, 2004.
(25) Spectral Database for Organic Compounds (SDBS): http://riodb01.ibase.aist.go.jp/sdbs/cgi-bin/cre_index.cgi.
(26) Frisch, M. J., et al. *Gaussian 03, Revision D.01*; Gaussian, Inc., Wallingford, CT, 2004.
(27) (a) Scott, A. P.; Radom, L. *J. Phys. Chem.* **1996**, *100*, 16502. (b) Sinha, P.; Boesch, S. E.; Gu, C.; Wheeler, R. A.; Wilson, A. K. *J. Phys. Chem. A* **2004**, *108*, 9213.
(28) Rode, J. E.; Dobrowolski, J. Cz. *J. Phys. Chem. A* **2006**, *110*, 207.
(29) Nash, J. J.; Kenttämaa, H. I.; Cramer, C. J. *J. Phys. Chem. A* **2005**, *109*, 10348.
(30) Van Geet, A. L. *Anal. Chem.* **1970**, *42*, 679.
(31) Exner, O. *Prog. Phys. Org. Chem.* **1973**, *10*, 411.
(32) Curtiss, L. A.; Redfern, P. C.; K. Raghavachari, K. *J. Chem. Phys.* **2005**, *123*, No. 124107.
(33) Kauzmann, W. *Quantum Chemistry*; Academic: San Diego, CA, 1957; p119.
(34) Wiest, O.; Montiel, D. C.; Houk, K. N. *J. Phys. Chem. A* **1997**, *101*, 8378.
(35) Seidl, E. T.; Schaefer, H. F., III. *J. Am. Chem. Soc.* **1991**, *113*, 5195.
(36) Cossio, F. P.; Roa, G.; Lecea, B.; Ugalde, J. M. *J. Am. Chem. Soc.* **1995**, *117*, 12306.
(37) (a) Carr, R. W.; Walters, W. D. *J. Phys. Chem.* **1963**, *67*, 1370. (b) Sirjean, B.; Glaude, P. A.; Ruiz-Lopez, M. F.; Fournet, R. *J. Phys. Chem. A* **2006**, *110*, 12693.
(38) (a) Ramhold, K.; Moll, K. K.; Roschka, E. *J. Prakt. Chem.* **1984**, *326*, 924. (b) Morales, G.; Martínez, R.; Ziegler, T. *J. Phys. Chem. A* **2008**, *112*, 3192.
(39) (a) *CRC Handbook of Chemistry and Physics*, 92nd ed.; Lide, D. R., Ed.; CRC Publishing Co.: Boca Raton, FL, 2011−2012; electronic edition http://hbcpnetbase.com; pp 5-20 and 5-21. (b) *CRC Handbook of Chemistry and Physics*, 92nd ed.; Lide, D. R., Ed.; CRC Publishing Co.: Boca Raton, FL, 2011−2012; electronic edition http://hbcpnetbase.com; pp 5-22, 5-24, and 5-27.
(40) Staudinger, H.; Göhring, O.; Schöller, M. *Chem. Ber.* **1914**, *47*, 40.

(41) Compernolle, F.; De Schryver, F. *J. Am. Chem. Soc.* **1975**, *97*, 3909.

(42) (a) Ebnöther, A.; Jucker, E.; Rissi, E.; Rutschmann, J.; Schreier, E.; Steiner, R.; Süess, R.; Vogel, A. *Helv. Chim. Acta* **1959**, *42*, 918. (b) Testa, E.; Fontanella, L.; Cristiani, G.; Mariani, L. *Helv. Chim. Acta* **1959**, *42*, 2370.

(43) (a) Fu, N.; Tidwell, T. T. *Tetrahedron* **2008**, *64*, 10465. (b) Cossio, F. P.; Arrieta, A.; Sierra, M. A. *Acc. Chem. Res.* **2008**, *41*, 925. (c) Lage, M. L.; Fernandez, I.; Sierra, M. A.; Torres, M. R. *Org. Lett.* **2011**, *13*, 2892.

(44) (a) Lecea, B.; Arrieta, A.; Lopez, X.; Ugalde, J. M.; Cossio, F. P. *J. Am. Chem. Soc.* **1995**, *117*, 12314. (b) Zhang, X.-h.; Geng, Z.-y. *J. Mol. Struct. (THEOCHEM)* **2010**, *955*, 33.

(45) Lim, C. C.; Xu, Z. P.; Huang, H. H.; Mok, C. Y.; Chin, W. S. *Chem. Phys. Lett.* **2000**, *325*, 433.

(46) James, T. L.; Wellington, C. A. *J. Am. Chem. Soc.* **1969**, *91*, 7743.

(47) Morao, I.; Lecea, B.; Arrieta, A.; Cossio, F. P. *J. Am. Chem. Soc.* **1997**, *119*, 816.

(48) Gong, L.; McAllister, M. A.; Tidwell, T. T. *J. Am. Chem. Soc.* **1991**, *113*, 6021.

(49) (a) Scott, A. P.; Radom, L. *Intl. J. Mass Spectrom. Ion Process.* **1997**, *160*, 73. (b) Simmie, J. M.; Metcalfe, W. K.; Curran, H. J. *ChemPhysChem* **2008**, *9*, 700.

(50) Bondi, H. *J. Phys. Chem.* **1964**, *68*, 441.

(51) Minh, T. D.; Strausz, O. P. *J. Am. Chem. Soc.* **1970**, *92*, 1766.

(52) Harkness, J. B.; Kistiakowsky, G. B.; Mears, W. H. *J. Chem. Phys.* **1937**, *5*, 682.